Friction
https://doi.org/10.1007/s40544-020-0483-z
ISSN 2223-7690
CN 10-1237/TH
RESEARCH ARTICLE

Tribological performance of various metal-doped carbon dots as water-based lubricant additives and their potential application as additives of poly(ethylene glycol)

Weiwei TANG, Xuejun ZHU, Yufeng LI*
School of Biological and Chemical Engineering, Panzhihua University, Panzhihua 617000, China
Received: 28 September 2020 / Revised: 29 October 2020 / Accepted: 21 December 2020

Abstract: Advances in nano-lubricant additives are vital to the pursuit of energy efficiency and sustainable development. Carbon dots (CDs) have been widely investigated in the domain of lubricant additives owing to their extraordinary tribological properties, in particular, their friction-reducing and anti-wear properties. Metal-doped CDs are a new type of CDs, and their friction-reducing and anti-wear properties are attracting increasing attention. Therefore, a series of CDs doped with various divalent metal ions have been successfully synthesized via one-pot pyrolysis. The tribological properties of the synthesized CDs as water-based lubricant additives are in the following order: Zn-CDs > Cu-CDs >> Mg-CDs > Fe-CDs > U-CDs. Specifically, adding 1.0 wt% of Zn-CDs into water-based lubricant results in 62.5% friction and 81.8% wear reduction. Meanwhile, the load-carrying capacity of the water-based lubricant increases from 120 N to at least 500 N. Zn-CDs as an additive have long service life. Additionally, anion-tuned Zn-CDs fabricated via anion exchange exhibit promise as lubricant additives for poly(ethylene glycol). Based on the results of wear scar surface analyses, it is discovered that tribochemical films, primarily composed of iron oxides, nitrides, metal carbonates, zinc oxides, zinc carbonates, organic compounds, and embedded carbon cores, formed on the rubbing surfaces with a thickness of approximately 270 nm when Zn-CDs are used as additives. This film combined with the "ball-bearing" and third-particle effects of Zn-CDs contributed to excellent lubrication performance.

Keywords: metal-doped carbon dots (CDs); water-based lubricant additives; tribological performance; lubrication mechanism

1 Introduction

In recent years, sustainable development has become a typically discussed theme worldwide and has increasingly attracted people's attention toward protecting the environment and energy saving, resulting in numerous advanced techniques being exploited. For example, novel environmentally friendly slurries have been developed and used widely in the semiconductor, microelectronics, and optoelectronics industries, consequently reducing pollution induced by traditional manufacturing and industries significantly [1–4]. Recently, nontoxic and eco-friendly carbon-based materials including fullerene, carbon nanotubes, graphene, onion-like carbon, nano-graphite, and nano-diamond have become research hotspots in material and chemical sciences. Carbon nanomaterials have attracted significant attention in many applications, such as photovoltaic devices, transparent and stealth devices, coatings, mano machines, sensors, and catalysts. Inspired by the extraordinary effect of modern lubrication techniques on energy saving and emission reduction, considerable efforts have been devoted to integrating modern lubrication techniques and carbon

* Corresponding author: Yufeng LI, E-mail: lyfpzh@163.com

materials [5–8]. Recently, Zhang et al. [9] realized macroscale superlubricity on a macroscale surface under a graphene-coated ball/microsphere/plate system. Their findings are conducive to bridging the application of superlubricity to the real world and can contribute positively to energy saving and reduction in carbon dioxide emission to the environment. In modern lubrication techniques, nano-based lubricant additives are vital for improving energy efficiency and protecting the environment. Carbon-based nanomaterials as additives that enhance the lubrication performances of base lubricants have been repeatedly confirmed in previous studies [10], owing to their excellent physicochemical and mechanical properties as well as unique self-lubricating properties.

Carbon dots (CDs), a promising zero-dimensional carbon-based nanomaterial (< 10 nm), are emerging as highly promising candidates for solving many forbidding scientific and technological problems in the fields of biology, material, and chemistry, owing to their favorable properties, such as negligible toxicity, distinguished optical properties, good biocompatibility, excellent electrical properties, superior chemical inertness, and favorable mechanical behaviors [11–14]. It is well known that CDs were serendipitously discovered during the purification of single-walled carbon nanotubes in 2004 and was first synthesized using the laser ablation method in 2006 [15, 16]. After the rapid development in the past nearly 20 years, dozens of methods (including hydrothermal, solvothermal, microwave, pyrolysis, and ultrasonic methods) and hundreds of precursors (e.g., egg, grass, orange juice, amino acids, milk, and carbon-based materials) have been established to fabricate this type of desirable nanomaterial [17–24]. Inspired by the progress achieved in the synthesis of CDs, researches have recently begun to exploit their novel properties for targeted applications by tuning and designing the structures of the surface group and/or carbon core [25, 26]. Two representative strategies, i.e., surface functionalization and elemental doping, have been employed frequently to achieve the aforementioned goals [27–29]. As the research progresses, the application range of CDs is expanding more widely based on various surface functionalization and doping techniques, e.g., sensors, drug delivery, solar cells, catalysis, and lubricant additives [30–35]. The latest application of CDs as high-performance lubricant additives has garnered increasing attention [36–40].

Seminal studies have demonstrated that CDs are generally assembled by carbon cores (classified into amorphous and crystalline states) and surface groups (such as oxygen-containing groups, organic small molecules, polymers, as well as ionic liquids and their derivatives) [41]. The most typically used strategy to enhance the properties and broaden the application of CDs is surface functionalization. Surface functionalization can endow CDs with many lubrication advantages, including small and uniform particle size, good dispersion stability, adjustable hydrophilicity, and robust chemical inertness, thereby improving the targeted application potential of CDs in nano-additives. For example, ionic liquids (ILs), aliphatic acids, and polymer-functionalized CDs can effectively enhance the lubrication performance of water-based lubricants, poly(ethylene glycol) (PEG), and poly-alpha-olefin [39, 42–44]. Many studies have suggested that the outstanding tribological properties of CDs are associated closely with their surface functional groups [45]. Briefly, the surface functional groups of CDs not only improved their various physicochemical properties, but also enhance their embedding stability and film-forming ability on the rubbing surfaces. Consequently, adjusting and controlling the surface functional groups of CDs has been considered as a primary approach for enhancing their tribological performance. Both theoretical and experimental results confirmed that doping the carbon cores of CDs with other elements is another effective approach for developing novel properties. Therefore, various doping methods with tens of elements, such as N, S, Si, B, and metallic elements, have been used to achieve the aforementioned goal [46–51]. The superior mechanical properties, high thermal stability, chemical inertness, and inherent self-lubricating effect of doped CDs distinguish them from conventional CDs, rendering them promising candidates for commercial nano-additives [52]. Meanwhile, the doped elements possess much higher reactivity toward the rubbing surface than traditional C and O; this is conducive to forming an effective tribochemical reaction film to alleviate the friction and wear of friction pairs.

In recent years, water-based lubricants have garnered more attention because of their numerous lubrication advantages such as low cost, high cooling capability, good noninflammability, and environmental friendliness [45, 53]. Water is a poor lubricant owing to its low viscosity, high surface tension, poor film-forming ability, and high corrosivity. A large number of studies have shown that the most efficient approach for enhancing the lubrication capacity of water-based lubricants, particularly the antiwear and friction-reducing performances, is by introducing the additional additives [54–56]. Owing to their abundant hydrophilic groups and facile preparation methods, IL-functionalized CDs (CD-ILs) have exhibited great potential as a type of commercial water-based lubricant additive [38, 40, 57, 58]. It is well known that the IL groups of CD-ILs can form many anchors on the metallic rubbing surfaces through electrostatic interactions, which is vital for reducing the friction and wear of rubbing surfaces. Nevertheless, the tribological performance of CD-ILs can be further improved. As previously mentioned, the introduction of metal ions into the carbon core may be an effective strategy for enhancing the tribological performance of CD-ILs owing to their good reactivity with rubbing surfaces and excellent self-repairing capability. However, relevant studies are scarce.

In this study, we synthesized a series of different divalent metal ions (such as Fe^{2+}, Cu^{2+}, Mg^{2+}, and Zn^{2+}) doped CD-ILs (abbreviated as metal-doped CDs) by directly pyrolyzing corresponding gluconates and ILs (1-aminopropyl-3-methyl-imidazolium bromide) for the first time. The morphologies and structures of the metal-doped CDs were analyzed in detail using various microscopic and spectroscopic techniques. The tribological functions of the metal-doped CDs as nano-additives of water-based lubricant (2.0 wt% of triethanolamine aqueous solution) were evaluated using a ball-on-plate type tribometer under a linear reciprocating mode. The effects of the type of doped metal ions, surface functional group, additive concentration, load, and test duration on the tribological properties of CDs were investigated in detail. Additionally, the potential application of anion-tuned Zn-CDs obtained via a simple anion exchange reaction between Br^- and $N(CF_3SO_2)_2^-$ in the water phase as a lubricant additive of PEG was exploited. Finally, the possible lubrication mechanism of metal-doped CDs was revealed using various surface analysis techniques, such as scanning electron microscopy (SEM), energy dispersive spectroscopy (EDS), X-ray photoelectron spectroscopy (XPS), and cross-section transmission electron microscopy (TEM).

2 Experimental

2.1 Chemicals

For this study, gluconates (including ferrous, copper, magnesium, and zinc gluconates) and 1-aminopropyl-3-methyl-imidazolium bromide ([AMIm][Br]) were purchased from Beijing Macklin Chemical Regent Co., Ltd. (China) and Lanzhou Institute of Chemical Physics (China), respectively. Bis(trifluoromethane)sulfonimide lithium ($LiN(CF_3SO_2)_2$, 98.5%) and triethanolamine (TEA, 99.5%) were obtained from Sigma–Aldrich Chemical Regent Co., Ltd. (China). Gluconic acid solution (50%) and PEG with an average molecular weight of 200 Da were provided by Beijing Macklin Chemical Regent Co., Ltd. (China). Petroleum ether (60%–90%) was purchased from Chengdu Kelong Chemical Regent Co., Ltd. (China). All chemicals were used as received without further purification, except for the gluconic acid solution. Before it was used, the water in the gluconic acid solution was removed via vacuum freeze-drying. Ultrapure water prepared using an OSJ-E-UP ultrapure water purifier (Oubolai, China) was used throughout the experiment.

2.2 Preparation of the metal-doped and undoped CDs

The metal-doped CDs were facilely synthesized using one-pot pyrolysis, i.e., directly pyrolyzing the precursors and functional reagents. The schematic diagram of the synthetic procedure is shown in Fig. 1. First, zinc gluconate (2.28 g, 0.005 mol) and [AMIm][Br] (3.30 g, 0.015 mol) were successively added into a three-neck flask (50 mL) fitted with a reflux condenser. Subsequently, the flask was rapidly placed in an oil bath and heated at 200 °C for 3 h under magnetic stirring and N_2 atmosphere. When the flask was cooled to the indoor temperature, 15 mL of ultrapure water

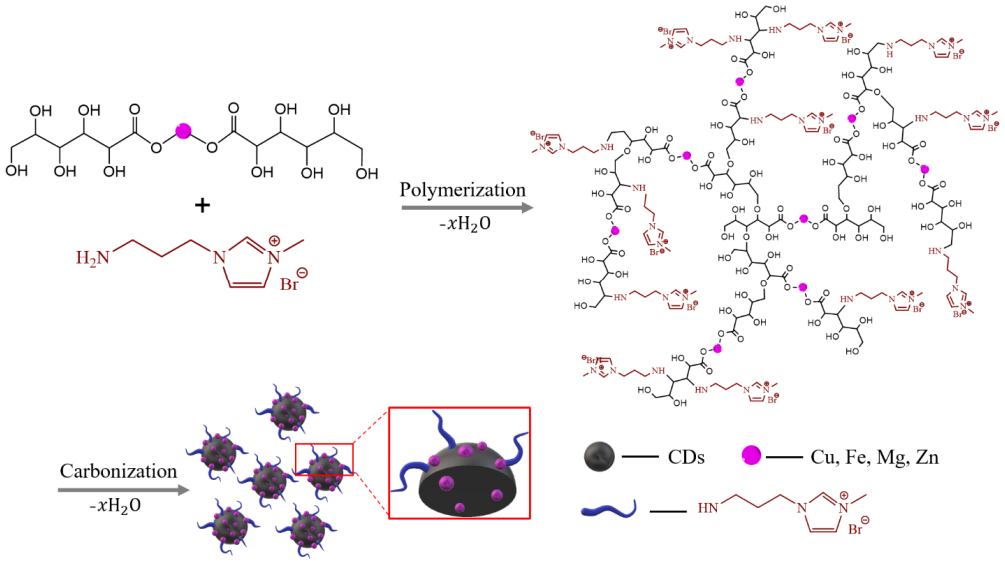

Fig. 1 Schematic illustration of synthesis procedure of metal-doped CDs.

was added under vigorous stirring. The obtained brownish–black dispersion was centrifuged at a rotating speed of 12,000 rpm for 10 min. The supernatant obtained via the centrifugation was transferred to a dialysis bag (molecular weight cutoff: 4,000 Da). The remaining molecular precursors and functional reagents in the supernatant were removed using the dialysis method as efficiently as possible. Finally, after dialysis, freezing, and drying, Zn-doped CD-ILs (simplified as Zn-CDs) were obtained. Using the same procedures, Fe-CDs, Cu-CDs, and Mg-CDs were synthesized. As reference samples, undoped CDs (abbreviated as U-CDs) were fabricated by directly pyrolyzing 1.0 g of the dried gluconic acid and 3.3 g of [AMIm][Br] at 200 °C for 3 h.

Anion-tuned Zn-CDs were prepared by an anion-exchange reaction in the water phase. Briefly, a predetermined amount of $LiN(CF_3SO_2)_2$ was added slowly to the Zn-CDs aqueous dispersion under vigorous stirring until the dispersion became colorless and transparent, reflecting that the Br^- on the surfaces of Zn-CDs was gradually replaced by $N(CF_3SO_2)_2^-$. The brownish–black precipitate, i.e., the anion-tuned Zn-CDs, was obtained and dried at 60 °C under vacuum for 48 h.

2.3 Characterization

TEM and high-resolution TEM (HR-TEM) images were obtained using a Tecnai G2 F20 S-TWIN system at an accelerating voltage of 200 kV. Fourier transform infrared (FTIR) spectra were recorded at wavenumbers in the 500–4,000 cm^{-1} range on a WQF-520 spectrophotometer using the KBr pellet technique. X-ray diffraction (XRD) patterns were obtained using a D8 Advance X-ray diffractometer with a wavelength (λ) of 0.15418 nm. XPS measurements were conducted using an ESCALAB 250 photoelectron spectrophotometer with a monochromatized Al Kα X-ray source (1,486.71 eV). Thermogravimetric analyses (TGA) were performed on a STA449F3 thermogravimetric analyzer under nitrogen flow at a heating rate of 10 °C/min from 40 to 700 °C. Additionally, the particle sizes of the CDs were determined using a Nicomp 380 dynamic light scattering particle size analyzer. Photographs of the CDs dispersions were obtained using a Canon camera (EOS 550) under sunlight.

2.4 Tribological tests

Tribological tests were performed on a UMT-3 tribometer (Bruker, USA) in the ball-on-plate reciprocating mode. In particular, a commercially available AISI-52100 steel ball (12.7 mm in diameter and hardness of 59–61 HRC) slid reciprocally against a low-stationary AISI-52100 steel plate (50 mm × 40 mm × 3 mm in size and 59–61 HRC in hardness). The steel plate was mounted in a holder and connected through a lever coupled with a friction force transducer. The friction coefficients were automatically recorded

using a computer coupled with a high-sensitivity sensor. To obtain convincing mean friction coefficient and mean wear volume values with an error bar, each test was conducted thrice under the following conditions: load, 40–500 N; duration, 20–120 min; frequency, 5 Hz; amplitude, 5 mm; ambient temperature and humidity. The mean friction coefficient value was calculated as the average of all data points on the friction coefficient curve, considering the error bars.

2.5 Wear scar surface analyses

After the tribological tests were performed, the wear scar surfaces of the lower plates were adequately washed using petroleum ether (60%–90%) under ultrasonic treatment for 10 min. The width, depth, wear volume, two-dimensional (2D) profile, and three-dimensional (3D) morphology of the wear scars of the lower plates were recorded using a Bruker Contour GT-K 3D optical microscope. The morphology and elemental composition of the wear scar surfaces were obtained via SEM coupled with EDS, XPS, and Raman spectroscopy. To confirm the tribochemical film on the wear scar surface, an ultrathin cross-section was extracted from the wear scar of the lower plate using focused ion beam; subsequently, it was characterized using TEM coupled with EDS.

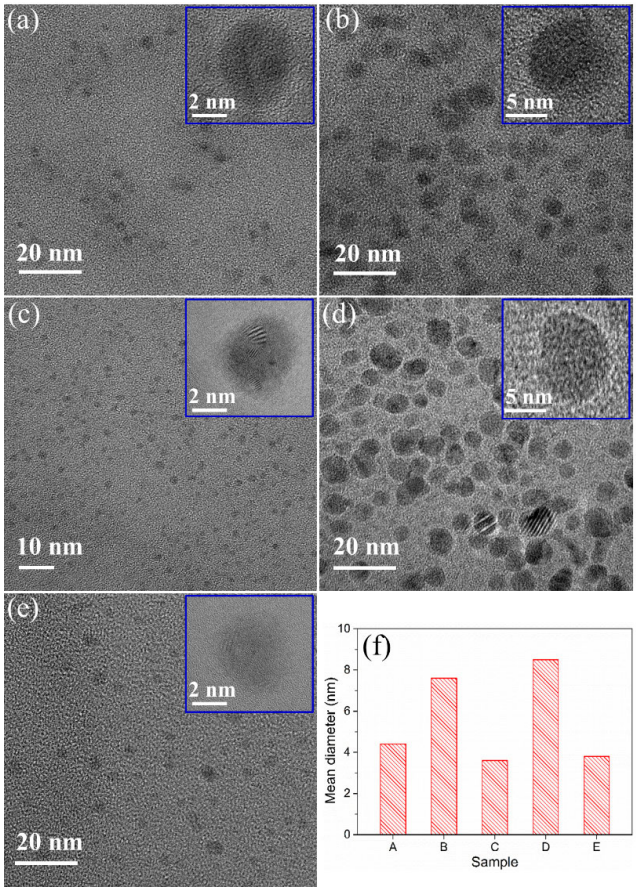

Fig. 2 TEM and HR-TEM (insets) images of (a) U-CDs, (b) Fe-CDs, (c) Cu-CDs, (d) Mg-CDs, and (e) Zn-CDs. (f) Particle size distributions of U-CDs (A), Fe-CDs (B), Cu-CDs (C), Mg-CDs (D), and Zn-CDs (E).

3 Results and discussion

3.1 Characterization

As illustrated in Figs. 2(a)–2(e), the TEM images demonstrated that all five CDs possessed pseudo-spherical shapes and uniform size distributions. Figure 2(f) shows that the average particle sizes of the U-CDs, Fe-CDs, Cu-CDs, Mg-CDs, and Zn-CDs were 4.4, 7.8, 3.6, 8.6, and 3.8 nm, respectively, implying that the various CDs were successfully synthesized via one-pot pyrolysis. Additionally, a clear difference in particle size was observed, i.e., the average particle sizes of the Fe-CDs and Mg-CDs were nearly twice those of the Cu-CDs and Zn-CDs, indicating the importance of the doped metal ions in controlling the size of the carbon cores. The HR-TEM images (insets of Figs. 2(a)–2(e)) show that all the CDs were almost amorphous in structure, which is the characteristic of CDs synthesized via the bottom-up strategy. This conclusion was further confirmed by the XRD patterns shown in Fig. 3(a). The only peak centered at 21.2°, corresponding to the (002) lattice plane of graphite, was broad and short, further revealing the poor crystallinity of the CDs above.

FTIR spectra were obtained to reveal the surface information of the fabricated CDs. As shown in Fig. 3(b), the peaks centered at 3,424, 1,725, 1,629, 1,386, 1,113, and 755 cm^{-1} can be assigned to the stretching vibrations of –OH and C=O, deformation vibrations of N–H, symmetric vibrations of C–H, stretching vibrations of C–O, and deformation vibrations of =C–H, respectively, indicating that the U-CDs were covalently capped by many oxygen-containing groups and [AMIm][Br] molecules. The FTIR spectra of the metal-doped CDs were similar to those of the

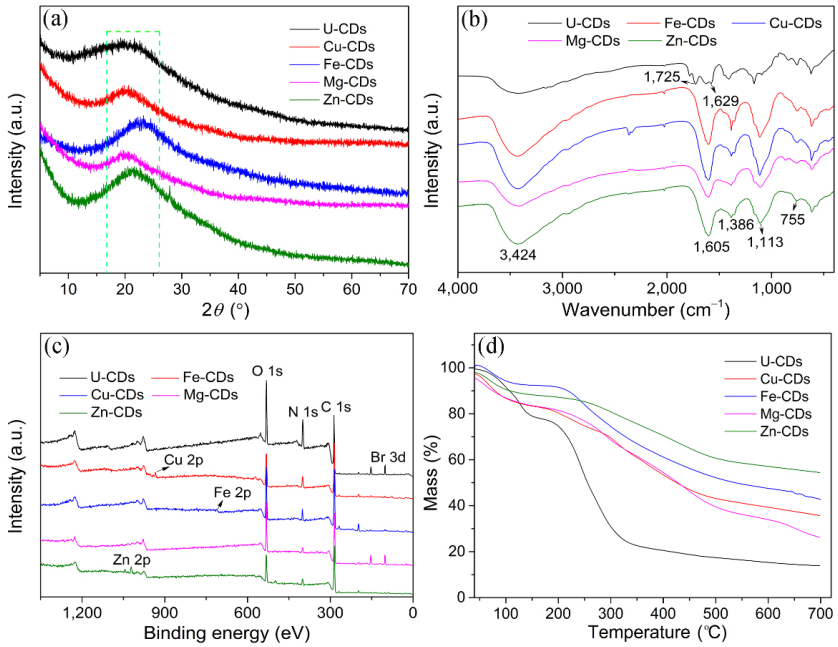

Fig. 3 (a) XRD patterns, (b) FTIR spectra, (c) XPS spectra, and (d) TGA curves of U-CDs, Fe-CDs, Cu-CDs, Mg-CDs, and Zn-CDs.

U-CDs. Compared with the spectrum of the U-CDs, the stretching vibration peak of C=O (1,725 cm^{-1}) disappeared in the spectra of the metal-doped CDs. Meanwhile, the stretching vibration peak of C=C shifted from 1,629 to 1,605 cm^{-1}, demonstrating that the surfaces of metal-doped CDs were abundant in the oxygen-containing groups and [AMIm][Br] molecules despite the reduced amount of oxygen-containing groups containing C=O.

The full-scan XPS spectra shown in Fig. 3(c) indicate that the U-CDs were primarily composed of C, H, O, and N as well as a trace amount of Br. The detailed elemental compositions of the U-CDs are listed in Table S1 in the Electronic Supplementary Material (ESM). Based on the corresponding atomic molar ratios of the CDs, their composition formula can be expressed as $C_{5.63}N_{0.81}H_{7.21}Br_{0.01}O_{0.79}$. In Fig. S1 in the ESM, the C–N (286.2 eV for C 1s, 399.5 eV for N 1s), O=C–N/C=O (288.5 eV for C 1s, 531.1 eV for O 1s), and N–H_2 (400.4 eV for N 1s) bonds can be observed in the HR elemental XPS spectra of U-CDs, further confirming that the [AMIm][Br] molecules were covalently grafted onto the surface of U-CDs by amido bonds. In addition to C, H, O, N, and Br, slight amounts of Fe, Cu, Mg, and Zn were discovered in the Fe-CDs, Cu-CDs, Mg-CDs, and Zn-CDs, suggesting that various metal ions were successfully doped into the carbon cores. The composition formulas of the Fe-CDs, Cu-CDs, Mg-CDs, and Zn-CDs can be expressed as $Fe_{0.09}C_{5.48}N_{0.51}H_{3.88}Br_{0.004}O_{1.13}$, $Cu_{0.07}C_{5.21}N_{0.78}H_{4.08}Br_{0.004}O_{1.1}$, $Mg_{0.15}C_{5.08}N_{0.39}H_{4.75}Br_{0.007}O_{1.54}$, and $Zn_{0.09}C_{5.86}N_{0.54}H_{2.86}Br_{0.003}O_{0.83}$, respectively (Table S1 in the ESM). As shown in Figs. S2–S5 in the ESM, the HR elemental XPS spectra of the Fe-CDs, Cu-CDs, Mg-CDs, and Zn-CDs can be deconvoluted into one or more peaks belonging to specific elemental species, verifying that the CDs were doped with various metal ions in the carbon cores and capped by oxygen-containing groups and [AMIm][Br] molecules on their surfaces.

The thermal stability of the various CDs was evaluated via TGA. As shown in Fig. 3(d), the TGA curve of the U-CDs shows a distinct weight loss below 350 °C, attributable to the evaporation of absorbed water and the thermal decomposition of surface functional groups. The TGA curves of the U-CDs and metal-doped CDs differed. All of the metal-doped CDs indicated two distinct weight loss ranges below 120 °C and within 200–500 °C because of the evaporation of absorbed water as well as the decomposition and volatilization of surface functional groups, respectively. In addition, the thermal residue fraction of the U-CDs, Fe-CDs, Cu-CDs, Mg-CDs, and Zn-CDs were approximately 14.1, 35.4, 42.6, 26.2 and 53.5 wt% at 700 °C, respectively, confirming that many

metal ions were immobilized onto the surfaces and embedded into the interior of the carbon cores. These fascinating findings indicate that the thermal stability of CDs can be improved substantially by introducing metal ions into their carbon cores, and the contents of various metal ions in the corresponding metal-doped CDs differed.

3.2 Dispersion stability of various CDs in water-based lubricant and anion-tuned Zn-CDs in PEG

It is well known that the good dispersion stability of nanoparticles in base lubricants is a vital prerequisite for their application as lubricant additives. Hence, all the synthesized CDs were quantitatively dispersed into the water-based lubricant (2.0 wt% of TEA aqueous solution) via ultrasonic treatment for 10 min. The dispersion stability of various CDs in the water-based lubricant (1.0 wt%) was intuitively evaluated using a convenient still-setting method. Figure 4(a) shows that all the CDs indicated good dispersion in water-based lubricants after preparation. No agglomerates or precipitates were observed at the bottom of the container (Fig. 4(b)), even when the dispersion was stored for three months, revealing the excellent dispersion stability of the synthesized CDs in the water-based lubricants. Meanwhile, the dispersion stability of anion-tuned Zn-CDs in PEG was high because the surfaces of the anion-tuned Zn-CDs were surrounded by many $N(CF_3SO_2)_2^-$ ions, which demonstrated good compatibility with PEG. Additionally, the dispersion stabilities of the prepared CDs in the water-based lubricants and PEG were evaluated using dynamic light scattering. As shown in Fig. S6 in the ESM, the average particle sizes of the U-CDs, Fe-CDs, Cu-CDs, Mg-CDs, Zn-CDs, and anion-tuned Zn-CDs were 4.6, 8.3, 3.7, 8.6, 4.9, and 7.5 nm, respectively, when the dispersions were allowed to stand for three months, further reflecting the outstanding dispersion stability of the synthesized CDs in the base lubricant.

3.3 Tribological properties of various CDs

Doped-metal ions should significantly affect the tribological properties of CDs, similarly to their physicochemical properties. Hence, under the same conditions, the tribological functions of the Fe-CDs, Cu-CDs, Mg-CDs, and Zn-CDs as water-based additives were compared. Figure 5(a) shows that the friction coefficient curves of the dispersions were visibly lower than those of the water-based lubricant, reflecting the distinguished friction-reducing performance of the metal-doped CDs. Based on the mean friction coefficients and wear volumes of the water-based lubricants and various CDs dispersions, as shown in Fig. 5(b), the friction-reducing and anti-wear performance sequence was Zn-CDs > Cu-CDs >> Mg-CDs > Fe-CDs. Specifically, the mean friction coefficient and wear volume of the Zn-CDs dispersion were 56.8% and 73.5%, 30.7% and 49.0%, and 54.7% and 68.7% lower than those of the Fe-CDs, Cu-CDs, and Mg-CDs dispersions (1.0 wt%), respectively. This result illustrates that the lubrication performance of the metal-doped CDs can be tuned by altering the species of the doped metal ions. A series of contrast tests were performed to further highlight the superiority of the Zn-CDs. As shown in Fig. 5(c), although the [AMIm][Br]

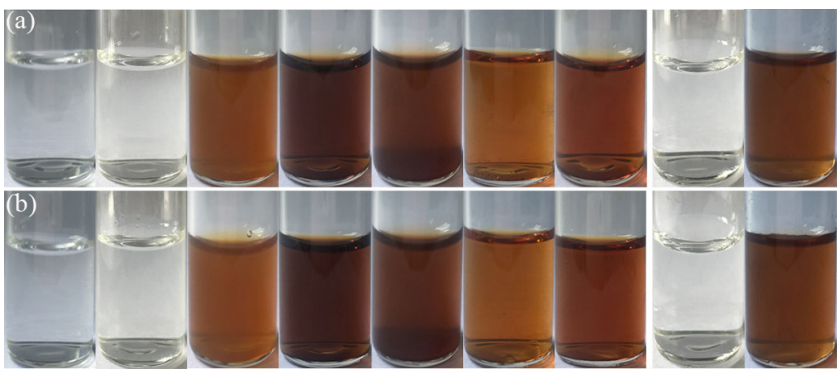

Fig. 4 Photographs of water-based lubricant, water-based lubricant containing 1.0 wt% [AMIm][Br], CDs, Fe-CDs, Cu-CDs, Mg-CDs, Zn-CDs, and PEG and PEG containing 0.15 wt% of anion-tuned Zn-CDs (from left to right) (a) after preparation and (b) standing for three months.

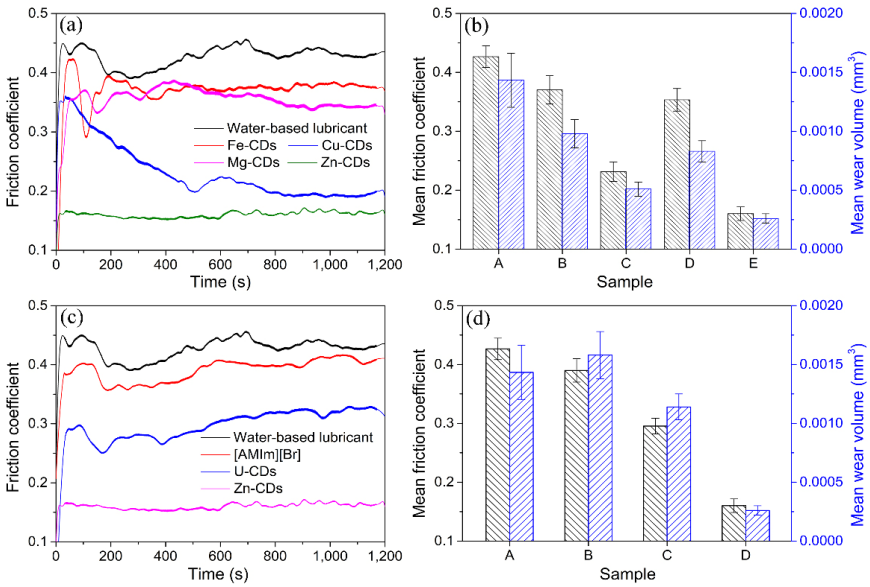

Fig. 5 (a) Friction coefficient curves (smoothed) of water-based lubricant, Fe-CDs, Cu-CDs, Mg-CDs, and Zn-CDs dispersions (1.0 wt%). (b) Mean friction coefficients and wear volumes of lower plates lubricated by water-based lubricant (A), Fe-CDs (B), Cu-CDs (C), Mg-CDs (D), and Zn-CDs (E) dispersions. (c) Friction coefficient curves (smoothed) of water-based lubricant, [AMIm][Br] solution, U-CDs, and Zn-CDs dispersions (1.0 wt%). (d) Mean friction coefficient and wear volume of lower plates lubricated by water-based lubricant (A), [AMIm][Br] solution (B), U-CDs (C), and Zn-CDs (D) dispersions. (Test conditions: 5 Hz, 20 min, 40 N, room temperature, and ambient humidity)

and U-CDs as additives (1.0 wt%) can effectively improve the friction-reducing performance of the water-based lubricant; however, the performance is still much weaker than that of the Zn-CDs. The Zn-CDs dispersion shows a 45.8%–58.9% decrease in friction and 77.2%–83.5% decline in wear compared with those of the [AMIm][Br] solution and U-CDs dispersion (Fig. 5(d)), demonstrating that the excellent tribological performance of the Zn-CDs might be closely associated with their carbon cores embedded by Zn ions rather than the surface [AMIm][Br] groups.

The effects of additive concentration (c, wt%) and load on the tribological properties of Zn-CDs were further investigated owing to their tremendous superiority over other types of CDs. Figure 6(a) shows the friction coefficient curves of Zn-CDs dispersions with various c values being markedly smoother and lower than those of the water-based lubricant, wherein the water-based lubricant containing 1.0 wt% Zn-CDs demonstrated the lowest friction coefficient curve, suggesting that an optimal c exists for Zn-CDs in the water-based lubricant. As shown in Fig. 6(b), the mean friction coefficient and wear volume of the lower plates first decreased significantly and then increased slightly as c increased, further confirming an optimal c of 1.0 wt% in this study. After adding 1.0 wt% Zn-CDs, the mean friction coefficient and wear volume of the water-based lubricant reduced by 62.5% and 81.8%, respectively, exhibiting the best friction-reducing and anti-wear performances. Figure 7 shows that the load-carrying capacity of the water-based lubricant can be significantly enhanced from 120 N to at least 500 N when only 1.0 wt% of Zn-CDs were introduced, which is an extremely rare value in water lubrication. The mean friction coefficients of the water-based lubricant and the Zn-CDs dispersion decreased slightly when the load increased (Fig. 7(a)), whereas the mean wear volumes exhibited the opposite behavior (Fig. 7(b)). These results indicate that the Zn-CDs exhibited outstanding friction-reducing and anti-wear performances under a wide load range of 40–500 N.

The lifetime of nano-lubricant additives significantly affects the performances of practical applications. In this study, the lifetime of Zn-CDs was assessed by prolonging the duration of the friction test from 20 to 120 min and increasing the load from 40 to 80 N. Figure 8(a) shows that the friction coefficient curve of the water-based lubricant first increased slightly and

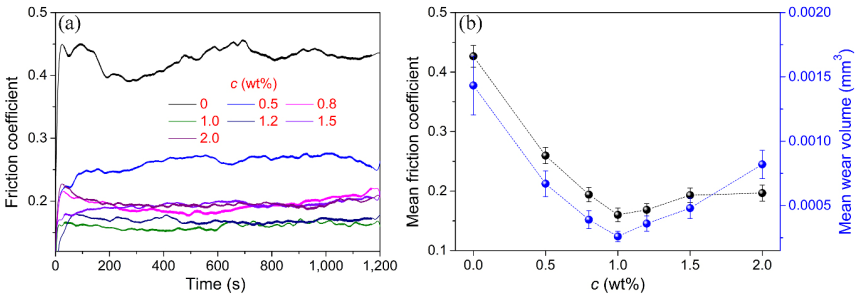

Fig. 6 (a) Friction coefficient curves (smoothed) of Zn-CDs dispersions with various *c*; (b) mean friction coefficient and wear volume of lower plates lubricated by Zn-CDs dispersions as a function of *c*. (Test conditions: 5 Hz, 20 min, 40 N, room temperature, and ambient humidity)

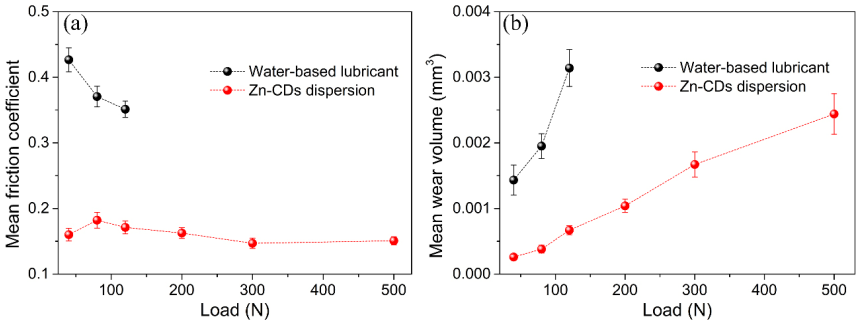

Fig. 7 (a) Mean friction coefficient and (b) mean wear volume of lower plates lubricated by water-based lubricant and Zn-CDs dispersion as a function of load. (Test conditions: 5 Hz, 20 min, 40–500 N, room temperature, and ambient humidity)

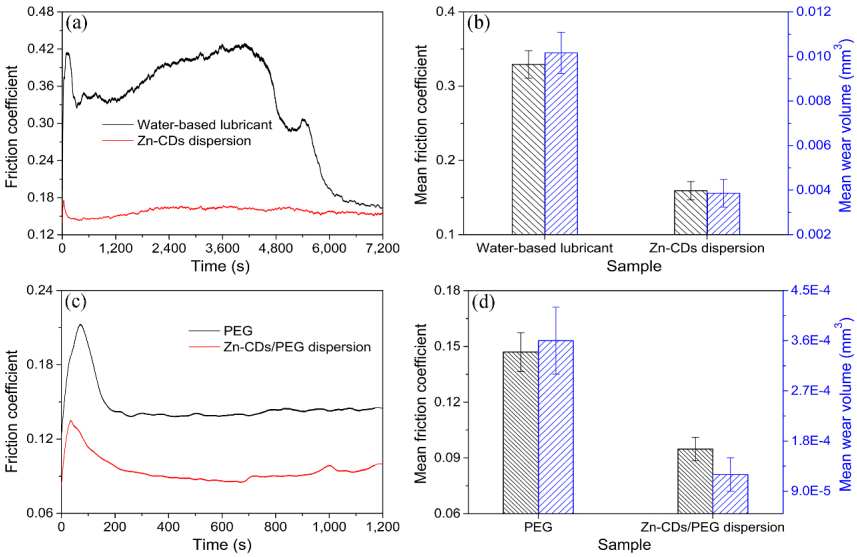

Fig. 8 (a) Friction coefficient curves; (b) mean friction coefficient and wear volume of lower plates lubricated by water-based lubricant and 1.0 wt% Zn-CDs dispersion. (Test conditions: 5 Hz, 120 min, 80 N, room temperature, and ambient humidity). (c) Friction coefficient curves; (d) mean friction coefficient and wear volume of lower plates lubricated by PEG and 0.15 wt% Zn-CDs/PEG dispersion. (Test conditions: 5 Hz, 20 min, 100 N, room temperature, and ambient humidity)

then declined significantly as time progressed, whereas the Zn-CDs dispersion (1.0 wt%) exhibited a stable and good lubrication function throughout the entire friction process. The mean friction coefficient and wear volume (Fig. 8(b)) of the dispersion reduced by 51.7% and 62.3%, respectively, compared with those of the water-based lubricant. Hence, the Zn-CDs maintained their lubrication effect over long time

period at relatively high loads, i.e., Zn-CDs as water-based lubricant additives afford a long lifetime. The exploitation of CDs-based lubricant additives with favorable universality is crucial for their further development. In this study, the prepared Zn-CDs can be utilized as an additive of PEG via a facile anion exchange reaction between Br^- and $N(CF_3SO_2)_2^-$ [59]. As shown in Fig. 8(c), the friction coefficient curve of the anion-tuned Zn-CDs/PEG dispersion is much lower than that of pure PEG. Additionally, the mean friction coefficient and wear volume (Fig. 8(d)) of the pure PEG reduced significantly by 35.5% and 66.7%, respectively, when only 0.15 wt% of anion-tuned Zn-CDs were introduced, revealing the potential of anion-tuned Zn-CDs as high-performance lubricant additives for PEG.

3.4 Wear scar surface analyses and lubrication mechanism

To reveal the lubrication mechanism of the metal-doped CDs, the wear scars of the lower plates were analyzed using a 3D optical microscope, SEM coupled with EDS, XPS, and cross-sectional TEM characterization. Figure 9 shows the 3D morphologies and 2D profiles of wear scars of the lower plates lubricated by the water-based lubricant, U-CDs, and various metal-doped CDs dispersions (1.0 wt%). The wear scars lubricated by the water-based lubricant containing various metal-doped CDs were distinctly smaller than those of the water-based lubricant and U-CDs dispersion, directly indicating the importance of doped metal ions in enhancing the antiwear property of CDs. Specifically, Figs. 9(a) and S7(a) in the ESM illustrate that the wear scar lubricated by the water-based lubricant was extremely wide and deep, with a large width of 281.99 μm and a depth of 4.32 μm. As shown in Figs. 9(b) and S7(b) in the ESM, although the width and depth of the wear scar were reduced to 264.99 and 3.38 μm, respectively, when 1.0 wt% U-CDs were added into the water-based lubricant, the wear scar of the U-CDs dispersion was still significantly larger than those of the Fe-CDs, Cu-CDs, Mg-CDs, and Zn-CDs dispersions (Figs. 9(c)–9(f) and S7(c)–7(f) in the ESM). Hence, the Zn-CDs dispersion demonstrated the best antiwear property. The wear scar width and depth of the Zn-CDs dispersion decreased by 43.1% and 34.7%, respectively, compared with those of the water-based lubricant.

Figure 10 shows the low- and HR-SEM images of the wear scar surfaces lubricated by the water-based lubricant and the water-based lubricant containing 1.0 wt% U-CDs, Fe-CDs, Cu-CDs, Mg-CDs, and Zn-CDs. As illustrated in Fig. 10(a), the wear scar lubricated by the water-based lubricant was large, with many wide and deep scratches, revealing the poor lubrication ability of the water-based lubricant. It can be speculated that the direct contact of the rubbing surfaces and the severe adhesive and corrosive wear occurred during the friction process. Compared with the water-based lubricant, the wear scars lubricated by the 1.0 wt% U-CDs and Mg-CDs dispersions (Figs. 10(b) and 10(e)) were smaller but rougher. Numerous of irregular and deep pits were observed in the HR-SEM images (shown by the blue arrow), implying that the abrasive wear caused by the aggregation of U-CDs and Mg-CDs was the dominating wear mode during the friction process. Figures 10(c) and 10(d) show many discontinuous flaky films on the wear scar surfaces lubricated by the Fe-CDs and Cu-CDs dispersions; they might have originated from the complicated tribochemical reaction between the metal-doped CDs and the metallic rubbing surfaces. By contrast, Fig. 10(f) shows that the wear scar lubricated by the Zn-CDs dispersion was particularly small and smooth, suggesting the excellent antiwear performance of the Zn-CDs. The metal-doped CDs exhibited better antiwear performance than the CDs. In addition, the Zn-CDs demonstrated the best antiwear performance in all of the metal-doped CDs, implying the importance of doped metal ions in improving the antiwear properties of CDs.

Figure 11 shows the selected area elemental maps of wear scar surfaces of the lower plates lubricated by the water-based lubricant, U-CDs, and metal-doped CDs dispersions (1.0 wt%). As shown in Fig. 11(a), uniform distributions of Fe, C, O and N were revealed on the wear scar surface lubricated by the water-based lubricant. The detected C, O, and N primarily originated from the adsorption of TEA molecules. In addition to the elements above, Br was detected on the wear scar surface lubricated by U-CDs dispersion. Meanwhile, the content of C was much higher than that of Br,

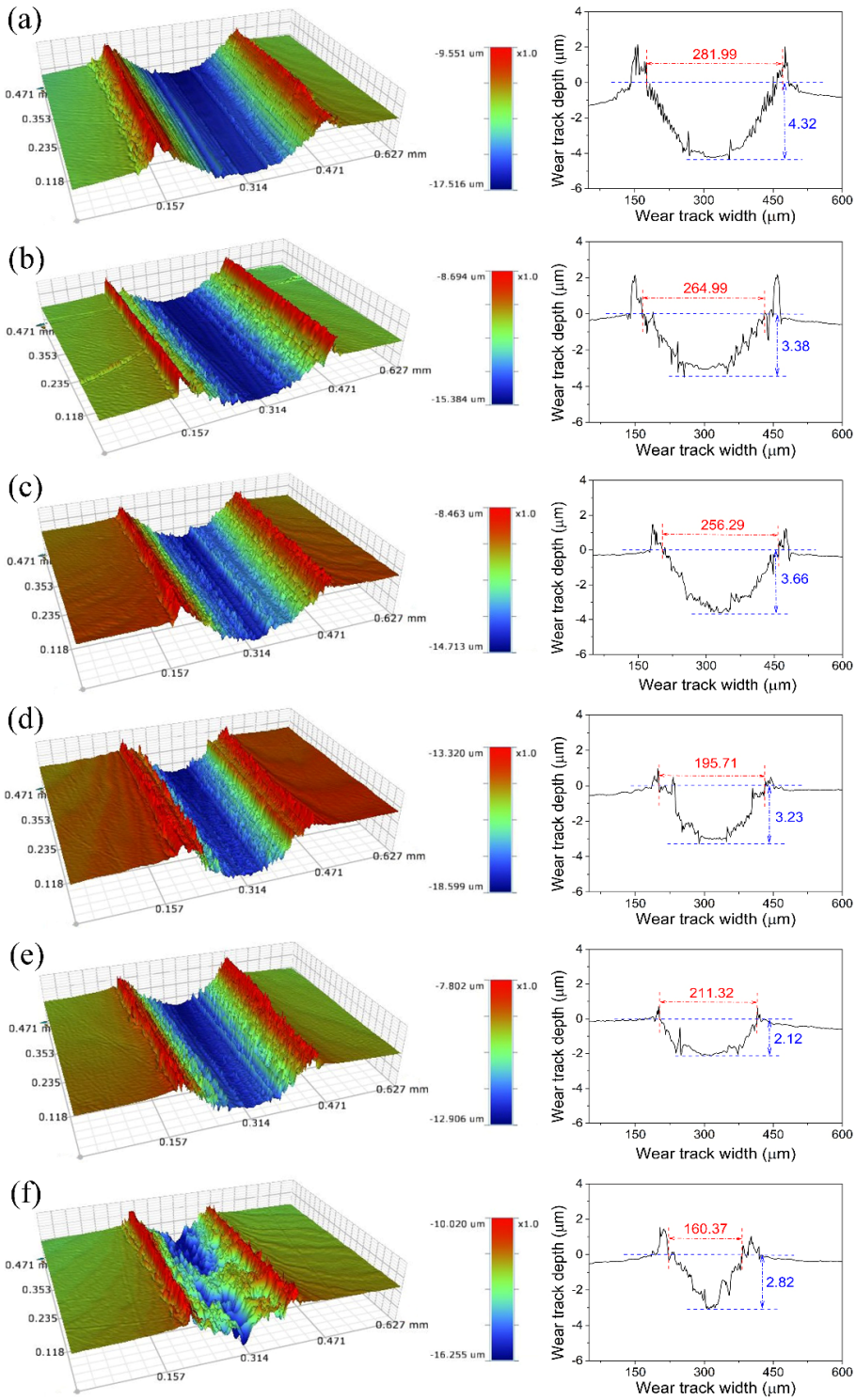

Fig. 9 3D morphologies and 2D profiles of lower plates lubricated by (a) water-based lubricant, (b) U-CDs, (c) Fe-CDs, (d) Cu-CDs, (e) Mg-CDs, and (f) Zn-CDs dispersions. (Test conditions: 5 Hz, 20 min, 40 N, room temperature, and ambient humidity)

implying the absorption and deposition of CDs on the rubbing surfaces (Fig. 11(b)). The elemental type of wear scar surface lubricated by Fe-CDs dispersion (Fig. 11(c)) was consistent with the wear scar surface lubricated by U-CDs dispersion, except that the content of O was higher. As illustrated in Figs. 11(d)–11(f), except for Fe, C, O, N, and Br, significant amounts of Cu, Mg, and Zn distributed uniformly on the wear

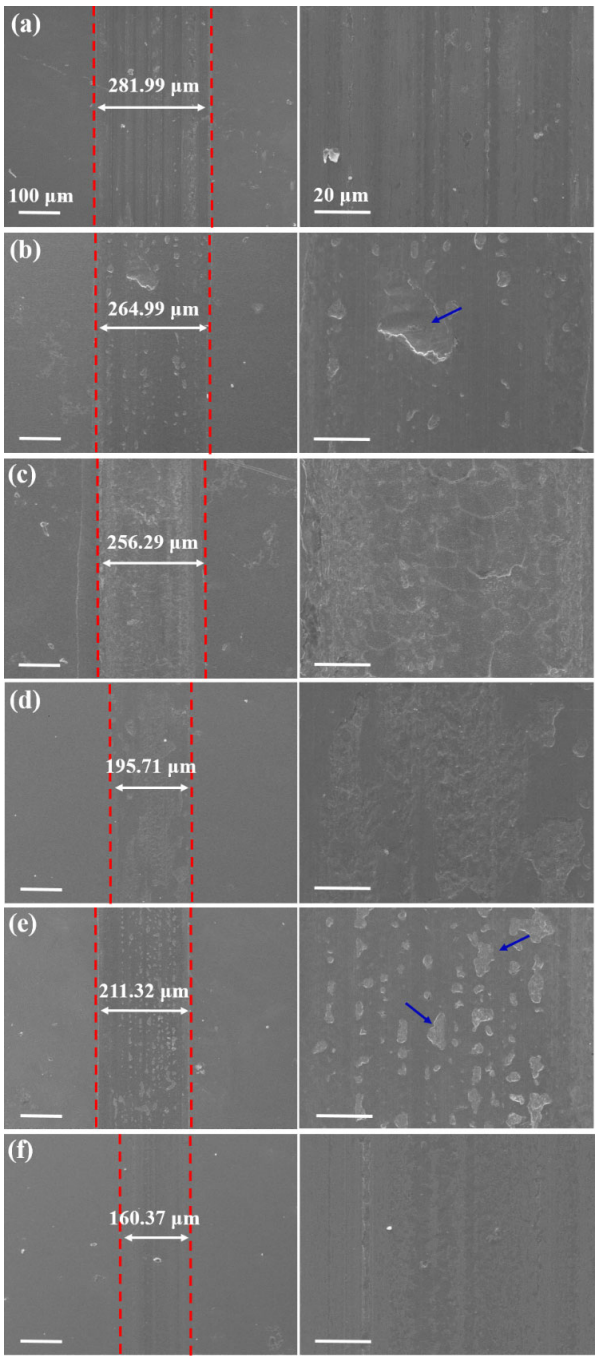

Fig. 10 Low- (left) and high-SEM (right) images of wear scars of lower plates lubricated by (a) water-based lubricant and 1.0 wt% (b) U-CDs, (c) Fe-CDs, (d) Cu-CDs, (e) Mg-CDs, and (f) Zn-CDs dispersions. (Test conditions: 5 Hz, 20 min, 40 N, room temperature, and ambient humidity)

scar surfaces lubricated by 1.0 wt% Cu-CDs, Mg-CDs, and Zn-CDs dispersions, respectively, confirming that the CDs-based additives above were evenly distributed on the corresponding wear scar surfaces, and they participated in the formation of the boundary tribofilm. These findings were consistent with the full-scan XPS spectra of the wear scar surfaces shown in Fig. S8 in the ESM.

Figure 12 shows the HR elemental XPS spectra of wear scar surfaces lubricated by the water-based lubricant and Zn-CDs dispersion (1.0 wt%). As illustrated in Fig. 12(a), the HR Fe 2p, C 1s, O 1s, and N 1s spectra show that iron oxides (such as FeO and Fe_2O_3), metal nitrides, and organic compounds (composed of C, O, and N) were present on the wear scar surface lubricated by the water-based lubricant. It can be speculated that complex tribochemical reactions occurred when the wear scar was lubricated by the water-based lubricant. In addition to iron oxides, nitrides, and organic compounds, zinc oxides, zinc carbonates, and metal carbonates can be probed on the wear scar surface lubricated by the 1.0 wt% Zn-CDs dispersion (Fig. 12(b)); it was suggested that the tribochemical reactions between the rubbing surfaces and Zn-CDs occurred during the friction process. It can be concluded that doped Zn ions are indispensable in enhancing the tribological performance of CDs.

The cross-sectional TEM image depicted in Fig. 13(a) shows that a tight tribofilm with an average thickness of approximately 270 nm and an amorphous structure can be intuitively observed between the Pt layer and the steel substrate on the wear scar surfaces lubricated by the 1.0 wt% Zn-CDs dispersion. The HR-TEM image in Fig. 13(b) shows the tribofilm embedded with many nanocrystals (approximately 4 nm), which is highly consistent with the average particle size of the Zn-CDs. The lattice spacing of the nanocrystal was approximately 0.32 nm (Fig. 11(c)); hence, it belonged to the (110) facet of graphite. The abovementioned results indicate that the carbon cores of the Zn-CDs transformed from an amorphous to a crystalline state under boundary lubrication conditions with high frictional heat and high contact pressure, suggesting that the Zn-CDs participated in the formation of the boundary tribofilm [60]. This result is further supported by the Raman spectrum of the wear scar surface lubricated by the 1.0 wt% Zn-CDs dispersion. Two typical peaks appeared at 1,310 and 1,587 cm^{-1}, which were assigned to the disorder-induced D band and tangential G band, respectively (as shown in Fig. S9 in the ESM); this confirmed the formation of a carbon-based film on the surface of the wear scar. As shown

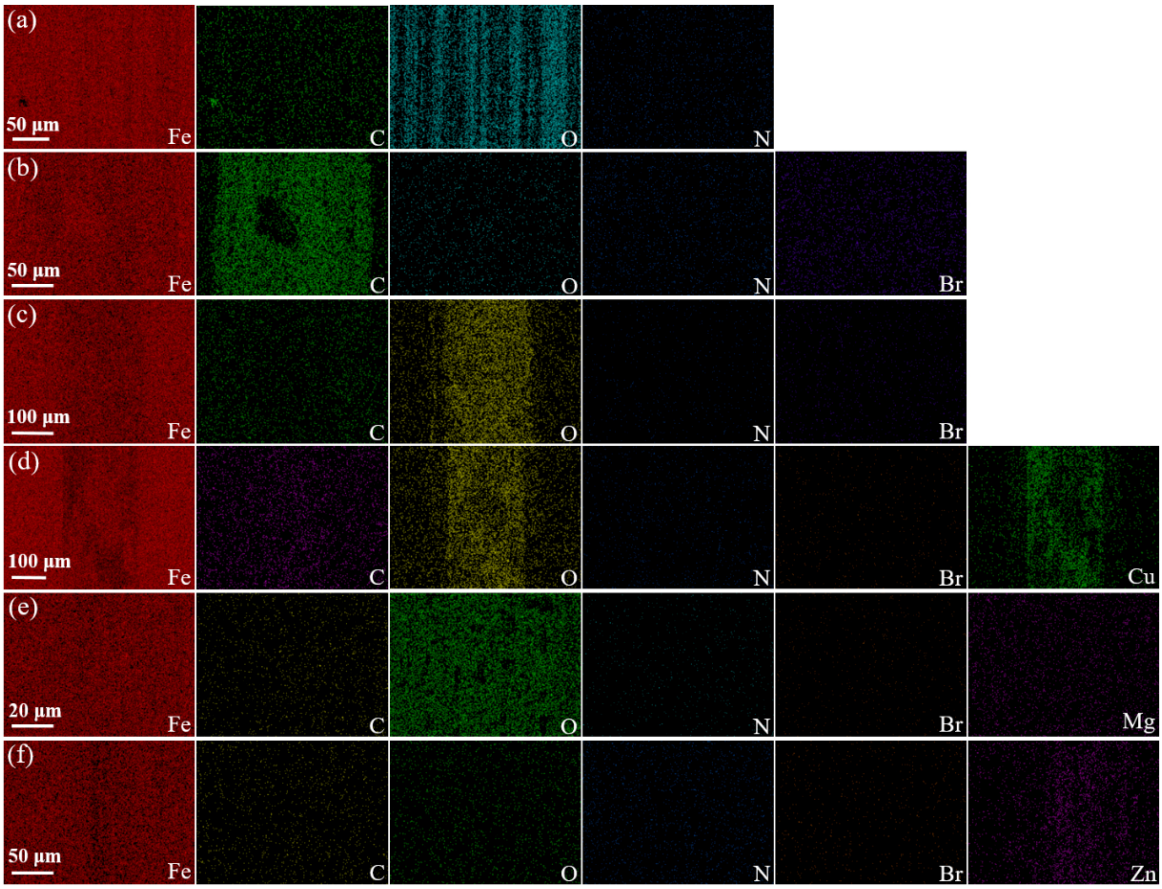

Fig. 11 Elemental maps of wear scar surfaces lubricated by (a) water-based lubricant and 1.0 wt% (b) U-CDs, (c) Fe-CDs, (d) Cu-CDs, (e) Mg-CDs, and (f) Zn-CDs dispersions. (Test conditions: 5 Hz, 20 min, 40 N, room temperature, and ambient humidity)

in Fig. 13(c), the EDS analyses of the selected area indicate that the tribofilm contained high amounts of C, O, N, and Zn as well as a low content of Fe, consistent with the XPS characterization and indicating that the tribofilm embedded with crystalline carbon cores was in fact a tribochemical film.

A more comprehensive insight into the lubrication mechanism of Zn-CDs is vital for not only tuning the lubrication function of the CDs by structure design, but also for extending the application of CDs in tribology. Based on the results of tribo-evaluations and wear scar surface analyses, a convincing lubrication mechanism of Zn-CDs as a water-based lubricant additive was established, as shown in Fig. 14. It is well known that the surfaces of a metallic friction pair will become positively charged as a result of low-energy electrons emitted from the contact points during the friction process. As previously mentioned, the [AMIm][Br] groups of the Zn-CDs not only endowed them with good dispersion stability in water-based lubricants, but also enabled many anchors to be formed on the rubbing surface by electrostatic interactions. First, the anchors significantly enhanced the absorption and embedding stability of the Zn-CDs on the rubbing surfaces. In addition, some complicated tribochemical reactions between the Zn-CDs and rubbing surfaces occurred and formed a tribochemical film with an average thickness of approximately 270 nm under the synergistic effect of high frictional heat and contact pressure. The formed tribochemical films embedded with many crystalline carbon cores were primarily composed of iron oxides, nitrides, metal carbonates, zinc oxides, zinc carbonates, and organic compounds containing C, O, N, and Br, which were indispensable for reducing the friction and wear by preventing the rubbing surfaces from direct contact. Moreover, the carbon cores doped with Zn ions in the tribochemical film can serve as "ball-bearings", which provide rolling, mending, and polishing effects to further alleviate friction and wear as well as repair the rubbing surfaces.

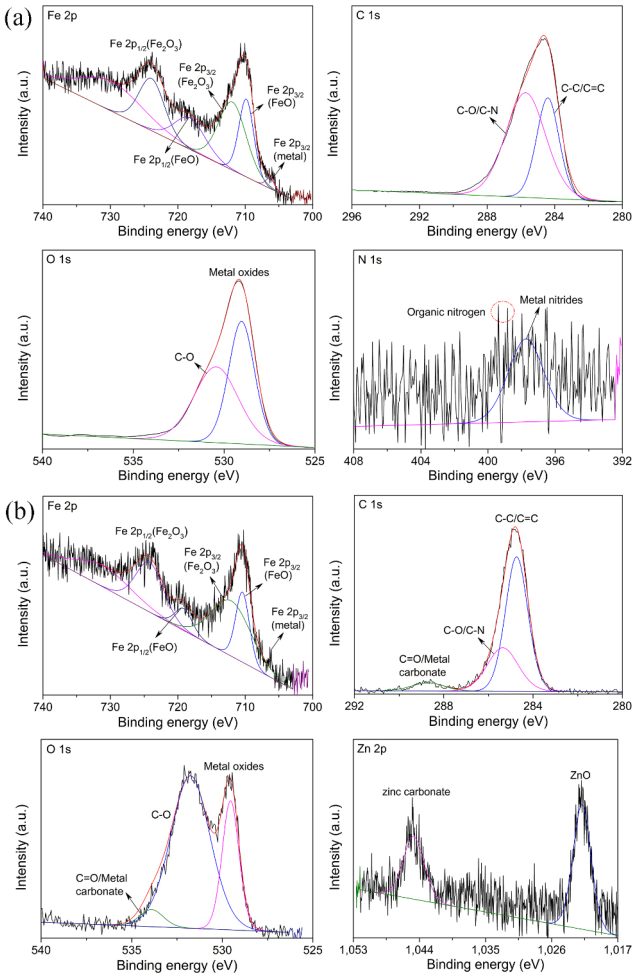

Fig. 12 (a) HR Fe 2p, C 1s, O 1s, and N 1s XPS spectra of wear scar of lower plate lubricated by water-based lubricant. (b) HR Fe 2p, C 1s, O 1s, and Zn 2p XPS spectra of wear scar of lower plate lubricated by Zn-CDs dispersion (1.0 wt%). (Test conditions: 5 Hz, 20 min, 40 N, room temperature, and ambient humidity)

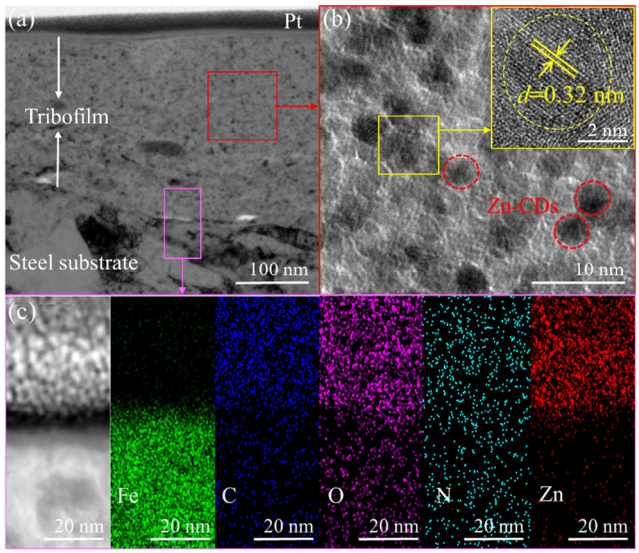

Fig. 13 (a, b) Bright-field cross-section TEM images and (c) EDS elemental maps of wear scar surface of lower plate lubricated by 1.0 wt% Zn-CDs dispersion. (Test conditions: 5 Hz, 20 min, 40 N, room temperature, and ambient humidity)

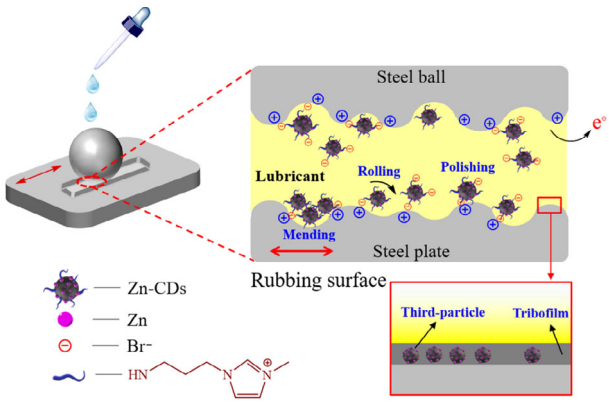

Fig. 14 Schematic illustration of lubrication mechanism of Zn-CDs as an additive of water-based lubricant.

4 Conclusions

U-CDs, Fe-CDs, Cu-CDs, Mg-CDs, and Zn-CDs with amorphous structures were successfully synthesized via the one-pot pyrolysis of the corresponding gluconates and [AMIm][Br]. The tribological behaviors of the abovementioned CDs as water-based lubricant additives were evaluated using the ball-on-plate reciprocating mode under steel/steel contact. The order of friction-reducing and anti-wear performances of various CDs were as follows: Zn-CDs > Cu-CDs >> Mg-CDs > Fe-CDs > U-CDs, indicating that doping the carbon cores of CDs with metal ions can significantly improve the tribological performance of CDs. An optimal *c* of 1.0 wt% was obtained for the Zn-CDs. At this *c*, the Zn-CDs reduced the friction coefficient and wear volume of the water-based lubricant by 32.3% and 56.4%, respectively. Meanwhile, the load-carrying capacity of the water-based lubricant increased from 120 N to at least 500 N, which is an extremely rare value in water lubrication. The lubrication functions of the Zn-CDs did not attenuate when the duration of the friction test was prolonged from 20 to 120 min and the load increased from 40 to 80 N. In addition, the Zn-CDs can be utilized as PEG additives by a simple anion exchange reaction between Br^- and $N(CF_3SO_2)_2^-$; the mean friction coefficient and wear volume of PEG were reduced by 35.5% and 66.7%, respectively, when only 0.15 wt% of anion-tuned

Zn-CDs were added. The wear scar surface analysis results indicated that Zn-CDs can react with the rubbing surface to form a robust tribochemical film with an average thickness of approximately 270 nm under local high frictional heat and high contact pressure, which directly prevents the rubbing surfaces from direct contact and hence significantly reduces friction and wear. Meanwhile, the Zn-CDs can serve as "ball-bearings" and third particles to further alleviate the friction and wear of rubbing surfaces.

Acknowledgements

This work was financially supported by the Science and Technology Innovation Seedling Project of Sichuan Province (No. 2020068).

Electronic Supplementary Material Supplementary material is available in the online version of this article at https://doi.org/10.1007/s40544-020-0483-z.

References

[1] Zhang Z Y, Liao L X, Wang X Z, Xie W X, Guo D M. Development of a novel chemical mechanical polishing slurry and its polishing mechanisms on a nickel alloy. *Appl Surf Sci* **506**: 144670 (2020)

[2] Zhang Z, Wang B, Zhou P, Kang R, Zhang B, Guo D. A novel approach of chemical mechanical polishing for cadmium zinc telluride wafers. *Sci Rep* **6**: 26891 (2016)

[3] Zhang Z Y, Cui J F, Zhang J B, Liu D D, Yu Z J, Guo D M. Environment friendly chemical mechanical polishing of copper. *Appl Surf Sci* **467**: 5–11 (2019).

[4] Zhang Z Y, Shi Z F, Du Y F, Yu Z J, Guo L C, Guo D M. A novel approach of chemical mechanical polishing for a titanium alloy using an environment-friendly slurry. *Appl Surf Sci* **427**: 409–415 (2018).

[5] Jariwala D, Sangwan V K, Lauhon L J, Marks T J, Hersam M C. Carbon nanomaterials for electronics, optoelectronics, photovoltaics, and sensing. *Chem Soc Rev* **42**(7): 2824–2860 (2013)

[6] Ravi S, Vadukumpully S. Sustainable carbon nanomaterials: Recent advances and its applications in energy and environmental remediation. *J Environ Chem Eng* **4**(1): 835–856 (2016)

[7] Peng Z, Liu X J, Zhang W, Zeng Z D, Liu Z F, Zhang C, Liu Y, Shao B B, Liang Q H, Tang W W, et al. Advances in the application, toxicity and degradation of carbon nanomaterials in environment: A review. *Environ Int* **134**: 105298 (2020)

[8] Guo L C, Zhang Z Y, Sun H Y, Dai D, Cui J F, Li M Z, Xu Y, Xu M S, Du Y F, Jiang N, et al. Direct formation of wafer-scale single-layer graphene films on the rough surface substrate by PECVD. *Carbon* **129**: 456–461 (2018)

[9] Zhang Z Y, Du Y F, Huang S L, Meng F L, Chen L L, Xie W X, Chang K K, Zhang C H, Lu Y, Lin C T, et al. Macroscale superlubricity enabled by graphene-coated surfaces. *Adv Sci* **7**(4): 1903239 (2020)

[10] Zhai W Z, Srikanth N, Kong L B, Zhou K. Carbon nanomaterials in tribology. *Carbon* **119**: 150–171 (2017)

[11] Lim S Y, Shen W, Gao Z Q. Carbon quantum dots and their applications. *Chem Soc Rev* **44**(1): 362–381 (2015)

[12] Wang Y F, Hu A G. Carbon quantum dots: Synthesis, properties and applications. *J Mater Chem C* **2**(34): 6921–6939 (2014)

[13] Yang S T, Cao L, Luo P G J, Lu F S, Wang X, Wang H F, Meziani M J, Liu Y F, Qi G, Sun Y P. Carbon dots for optical imaging *in vivo*. *J Am Chem Soc* **131**(32): 11308–11309 (2009)

[14] Chandra S, Das P, Bag S, Laha D, Pramanik P. Synthesis, functionalization and bioimaging applications of highly fluorescent carbon nanoparticles. *Nanoscale* **3**(4): 1533–1540 (2011)

[15] Xu X Y, Ray R, Gu Y L, Ploehn H J, Gearheart L, Raker K, Scrivens W A. Electrophoretic analysis and purification of fluorescent single-walled carbon nanotube fragments. *J Am Chem Soc* **126**(40): 12736–12737 (2004)

[16] Sun Y P, Zhou B, Lin Y, Wang W, Fernando K A S, Pathak P, Meziani M J, Harruff B A, Wang X, Wang H F, et al. Quantum-sized carbon dots for bright and colorful photoluminescence. *J Am Chem Soc* **128**(24): 7756–7757 (2006)

[17] Yan F Y, Zou Y, Wang M, Dai L F, Zhou X G, Chen L. Synthesis and application of the fluorescent carbon dots. *Prog Chem* **26**(1): 61–74 (2014).

[18] Wang W, Cheng L, Liu W G. Biological applications of carbon dots. *Sci China Chem* **57**(4): 522–539 (2014)

[19] Huang H, Xu Y, Tang C J, Chen J R, Wang A J, Feng J J. Facile and green synthesis of photoluminescent carbon nanoparticles for cellular imaging. *New J Chem* **38**(2): 784–789 (2014)

[20] Das Purkayastha M, Manhar A K, Das V K, Borah A, Mandal M, Thakur A J, Mahanta C L. Antioxidative, hemocompatible, fluorescent carbon nanodots from an "end-of-pipe" agricultural waste: Exploring its new horizon in the food-packaging domain. *J Agric Food Chem* **62**(20): 4509–4520 (2014)

[21] Chen X X, Jin Q Q, Wu L Z, Tung C, Tang X J. Synthesis and unique photoluminescence properties of nitrogen-rich quantum dots and their applications. *Angew Chem* **126**(46): 12750–12755 (2014)

[22] Tajik S, Dourandish Z, Zhang K Q, Beitollahi H, Le Q V, Jang H W, Shokouhimehr M. Carbon and graphene quantum dots: A review on syntheses, characterization, biological and sensing applications for neurotransmitter determination. *RSC Adv* **10**(26): 15406–15429 (2020)

[23] Wang B G, Liu X, Dai S S, Lu H S. α-Fe_2O_3 nanoparticles/porous g-C_3N_4 hybrids synthesized by calcinations of Fe-based MOF/melamine mixtures for boosting visible-light photocatalytic tetracycline degradation. *Chemistryselect* **5**(11): 3303–3311 (2020)

[24] Wang B G, Liu X, Duan W M, Dai S S, Lu H S. Visual and ratiometric fluorescent determination of Al^{3+} by a red-emission carbon dot-quercetin system. *Microchem J* **156**: (2020)

[25] Wang B G, Zhao B. Carbon dots/$CoFe_2O_4$ mesoporous nanosphere composites as a magnetically separable visible light photocatalyst. *Russ J Phys Chem* **93**(2): 393–399 (2019)

[26] Zhao B, Wang B G, Lu H S, Dai S S, Huang Z Y. Tuning the visible-light photocatalytic degradation activity of thin nanosheets constructed porous g-C_3N_4 microspheres by decorating ionic liquid modified carbon dots: Roles of heterojunctions and surface charges. *New J Chem* **43**(25): 10141–10150 (2019)

[27] Chen Y Y, Qin X, Yuan C L, Wang Y L. Switch on fluorescence mode for determination of l-cysteine with carbon quantum dots and Au nanoparticles as a probe. *RSC Adv* **10**(4): 1989– 1994 (2020)

[28] Dong Y Q, Wang R X, Li H, Shao J W, Chi Y W, Lin X M, Chen G N. Polyamine-functionalized carbon quantum dots for chemical sensing. *Carbon* **50**(8): 2810–2815 (2012)

[29] Wang B G, Liang Z, Tan H, Duan W M, Luo M N. Red-emission carbon dots-quercetin systems as ratiometric fluorescent nanoprobes towards Zn^{2+} and adenosine triphosphate. *Microchimica Acta* **187**(6): 1–9 (2020)

[30] Chen Y, Cao Y, Ma C, Zhu J J. Carbon-based dots for electrochemiluminescence sensing. *Mater Chem Front* **4**(2): 369–385 (2020)

[31] Luo X M, Bai P X, Wang X C, Zhao G H, Feng J Y, Ren H J. Preparation of nitrogen-doped carbon quantum dots and its application as a fluorescent probe for Cr(VI) ion detection. *New J Chem* **43**(14): 5488–5494 (2019)

[32] Ding L Y, Wang X T, Li J L, Huang J, Li Z J. Synthesis of fluorescent carbon quantum dots and their application in the plant cell imaging. *J Wuhan Univ Technol-Mater Sci Ed* **33**(6): 1546–1550 (2018)

[33] Wang R, Lu K Q, Tang Z R, Xu Y J. Recent progress in carbon quantum dots: synthesis, properties and applications in photocatalysis. *J Mater Chem A* **5**(8): 3717–3734 (2017)

[34] Ding H, Cheng L W, Ma Y Y, Kong J L, Xiong H M. Luminescent carbon quantum dots and their application in cell imaging. *New J Chem* **37**(8): 2515–2520 (2013)

[35] Ye M T, Cai T, Zhao L N, Liu D, Liu S G. Covalently attached strategy to modulate surface of carbon quantum dots: Towards effectively multifunctional lubricant additives in polar and apolar base fluids. *Tribol Int* **136**: 349–359 (2019)

[36] Mou Z H, Wang B G, Huang Z Y. Branched polyethyleneimine modified carbon nanoparticles as the effective additives of water lubrication. *Fuller Nanotub Car N* **27**(12): 899–906 (2019)

[37] Mou Z H, Wang B G, Huang Z Y, Lu H S. Ultrahigh yield synthesis of mesoporous carbon nanoparticles as a superior lubricant additive for polyethylene glycol. *Dalton Trans* **49**(16): 5283–5290 (2020)

[38] Mou Z H, Wang B G, Lu H S, Dai S S, Huang Z Y. Synthesis of poly(ionic liquid)s brush-grafted carbon dots for high-performance lubricant additives of polyethylene glycol. *Carbon* **154**: 301–312 (2019)

[39] Mou Z H, Wang B G, Lu H S, Quan H P, Huang Z Y. Branched polyelectrolyte grafted carbon dots as the high-performance friction-reducing and antiwear additives of polyethylene glycol. *Carbon* **149**: 594–603 (2019)

[40] Tang W W, Wang B G, Li J T, Li Y Z, Zhang Y, Quan H P, Huang Z Y. Facile pyrolysis synthesis of ionic liquid capped carbon dots and subsequent application as the water-based lubricant additives. *J Mater Sci* **54**(2): 1171–1183 (2019)

[41] Miao P, Han K, Tang Y G, Wang B D, Lin T, Cheng W B. Recent advances in carbon nanodots: synthesis, properties and biomedical applications. *Nanoscale* **77**(5): 1586–1595 (2015)

[42] Liu X, Huang Z Y, Tang W W, Wang B G. Remarkable

lubricating effect of ionic liquid modified carbon dots as a kind of water-based lubricant additives. *Nano* **12**(9): 1750108 (2017)

[43] Liu X, Chen Y. Synthesis of polyethylene glycol modified carbon dots as a kind of excellent water-based lubricant additives. *Fuller Nanotub Car N* **27**(5): 400–409 (2019)

[44] Ye M T, Cai T, Shang W J, Zhao L N, Zhang Y X, Liu D, Liu S G. Friction-induced transfer of carbon quantum dots on the interface: Microscopic and spectroscopic studies on the role of inorganic–organic hybrid nanoparticles as multifunctional additive for enhanced lubrication. *Tribol Int* **127**: 557–567 (2018)

[45] Tang J Z, Chen S Q, Jia Y L, Ma Y, Xie H M, Quan X, Ding Q. Carbon dots as an additive for improving performance in water-based lubricants for amorphous carbon (a-C) coatings. *Carbon* **156**: 272–281 (2020)

[46] Wang W P, Lu Y C, Huang H, Wang A J, Chen J R, Feng J J. Facile synthesis of N, S-codoped fluorescent carbon nanodots for fluorescent resonance energy transfer recognition of methotrexate with high sensitivity and selectivity. *Biosens Bioelectron* **64**: 517–522 (2015)

[47] Xue M Y, Zhang L L, Zou M B, Lan C Q, Zhan Z H, Zhao S L. Nitrogen and sulfur co-doped carbon dots: A facile and green fluorescence probe for free chlorine. *Sensor Actuat B: Chem* **219**: 50–56 (2015)

[48] Wu W T, Zhan L Y, Fan W Y, Song J Z, Li X M, Li Z T, Wang R Q, Zhang J Q, Zheng J T, Wu M B, et al. Cu–N dopants boost electron transfer and photooxidation reactions of carbon dots. *Angew Chem* **127**(22): 6640–6644 (2015)

[49] Chinigar A O, Shomali A, Valizadeh H. Boron/nitrogen co-doped carbon quantum dots as a high sensitive and selective fluorescent sensor for PO_4^{3-}-detection. *Org Commun* **13**(1): 9–18 (2020)

[50] Wang N, Fan H, Sun J C, Han Z W, Dong J, Ai S Y. Fluorine-doped carbon nitride quantum dots: Ethylene glycol-assisted synthesis, fluorescent properties, and their application for bacterial imaging. *Carbon* **109**: 141–148 (2016)

[51] Shan X Y, Chai L J, Ma J J, Qian Z S, Chen J R, Feng H. B-doped carbon quantum dots as a sensitive fluorescence probe for hydrogen peroxide and glucose detection. *Analyst* **139**(10): 2322–2325 (2014)

[52] Shang W J, Cai T, Zhang Y X, Liu D, Liu S G. Facile one pot pyrolysis synthesis of carbon quantum dots and graphene oxide nanomaterials: All carbon hybrids as eco-environmental lubricants for low friction and remarkable wear-resistance. *Tribol Int* **118**: 373–380 (2018)

[53] Meng Y G, Xu J, Jin Z M, Prakash B, Hu Y Z. A review of recent advances in tribology. *Friction* **8**(2): 221–300 (2020)

[54] Cui Y X, Ding M, Sui T Y, Zheng W, Qiao G C, Yan S, Liu X B. Role of nanoparticle materials as water-based lubricant additives for ceramics. *Tribol Int* **142**: 105978 (2020)

[55] Qiang R B, Hu L F, Hou K M, Wang J Q, Yang S R. Water-soluble graphene quantum dots as high-performance water-based lubricant additive for steel/steel contact. *Tribol Lett* **67**(2): 64–73 (2019)

[56] Hu Y W, Wang Y X, Wang C T, Ye Y W, Zhao H C, Li J L, Lu X J, Mao C L, Chen S J, Mao J M, et al. One-pot pyrolysis preparation of carbon dots as eco-friendly nanoadditives of water-based lubricants. *Carbon* **152**: 511–520 (2019)

[57] Wang B G, Tang W W, Liu X, Huang Z Y. Synthesis of ionic liquid decorated muti-walled carbon nanotubes as the favorable water-based lubricant additives. *Appl Phys A* **123**(11): 680 (2017)

[58] Wang B G, Tang W W, Lu H S, Huang Z Y. Hydrothermal synthesis of ionic liquid-capped carbon quantum dots with high thermal stability and anion responsiveness. *J Mater Sci* **50**(16): 5411–5418 (2015)

[59] Wang B G, Tang W W, Lu H S, Huang Z Y. Ionic liquid capped carbon dots as a high-performance friction-reducing and antiwear additive for poly(ethylene glycol). *J Mater Chem A* **4**(19): 7257–7265 (2016)

[60] Shi J Q, Zhu X Z, Sun K, Fang L. Movement pattern of an ellipsoidal nanoparticle confined between solid surfaces: theoretical model and molecular dynamics simulation. *Friction*: 1–12 (2020)

Weiwei TANG. He received his Ph.D. degree in chemical engineering and technology from Southwest Petroleum University, Chengdu, China, in 2019. He joined the School of Biological and Chemical Engineering at Panzhihua University in 2019. His current position is a lecturer. His research interests include nanomaterials, nanocomposites, and microtribology.

Xuejun ZHU. He received his Ph.D. degree in chemical engineering from Sichuan University, Chengdu, China, in 2008. He joined the School of Biological and Chemical Engineering at Panzhihua University in 1997. His current position is a professor. His research areas cover the mass transfer and separation, as well as fluidization technology.

Yufeng LI. He received his M.S. degree in applied chemistry from Southwest Petroleum University, Chengdu, China, in 2006, and his Ph.D. degree in material physics and chemistry from Sichuan University, Chengdu, China, in 2013, respectively. He joined the School of Biological and Chemical Engineering at Panzhihua University in 1997. His current position is a professor. His research areas cover the carbon materials, nanocomposites, and lithium-ion batteries.